nature communications

Article

https://doi.org/10.1038/s41467-025-62529-9

Computational identification of small molecules for increased gene expression by synthetic circuits in mammalian cells

Received: 6 September 2024

Accepted: 24 July 2025

Published online: 04 August 2025

Check for updates

M. Pisani[1], F. Calandra[1], A. Rinaldi[1], F. Cella[1,8], F. Tedeschi[1], I. Boffa[2], D. Vozzi[3], N. Brunetti-Pierri[2,4,5], A. Carissimo[6], F. Napolitano[7] & V. Siciliano[1]

Engineering mammalian cells with synthetic circuits drives innovation in next-generation biotherapeutics and industrial biotechnology. However, applications often depend on cellular productivity, which is constrained by finite cellular resources. Here, we harness computational biology to identify drugs that boost productivity without additional genetic modifications. We perform RNA-sequencing on cells expressing an incoherent feed-forward loop (iFFL), a genetic circuit that enhances operational capacity. To find drugs that mimic this effect, we use DECCODE (Drug Enhanced Cell COnversion using Differential Expression), an unbiased method that matches our transcriptional data with thousands of drug-induced profiles. Among the compound candidates, we select Filgotinib, that enhances expression of both transiently and stably expressed genetic payloads across various experimental scenarios and cell lines, including AAV and lentivirus transduction. Our results reveal cell-specific responses, underscoring the context dependency of small-molecule treatments. Altogether, we present a versatile tool for biomedical and industrial applications requiring enhanced productivity from engineered cells.

Mammalian cell engineering with synthetic circuits is a disruptive technology for the study of biological processes such as cancer treatment[1–3] cell differentiation[4], gene pathway elucidation[5] and evolution[6]. Over the years it has also gained clinical relevance for the production and test of biologics[7–9], such as recombinant proteins[10], viral vectors, virus-like particles and cell-based therapies[2,3,11,12]. At the core of these applications is the transient or stable expression of genetic payloads to facilitate rapid and robust genetic prototyping of synthetic circuits[8,13–15], and regulatory compliance in biomanufacturing.

We have recently shown that the dependence of gene expression on resources availability is detrimental to the operational capacity of the host cells[16–19] and therefore to therapeutics bioproduction and genetic circuits characterization. This issue was overlooked in the first wave of mammalian cell engineering but it is now being addressed with complementary approaches that span from the characterization of circuit-host cell interaction of different genetic modules (e.g., promoters, Kozak, PolyA)[19], which exhibit a cell-type dependent effect, to the implementation of biomolecular incoherent feed forward loops (iFFLs) controllers based on endoribonucleases or microRNAs (miRNAs)[17,18,20] that are portable and re-adaptable. Importantly, we found that in miRNA-iFFL the protein production rate increases by a mechanism of translational resource re-distribution[20] enhancing the operational capacity of the engineered cells. However, according to the specific design, they may

[1]Synthetic and Systems Biology lab for Biomedicine, Istituto Italiano di Tecnologia-IIT, Naples, Italy. [2]Telethon Institute of Genetics and Medicine (TIGEM), Pozzuoli, Italy. [3]Istituto Italiano di Tecnologia-IIT, Genoa, Italy. [4]Department of Translational Medicine, University of Naples "Federico II", Naples, Italy. [5]Scuola Superiore Meridionale (SSM, School of Advanced Studies), Genomics and Experimental Medicine Program, University of Naples Federico II, Naples, Italy. [6]Istituto per le Applicazioni del Calcolo "Mauro Picone", Consiglio Nazionale delle Ricerche (CNR), Naples, Italy. [7]Department of Science and Technology, University of Sannio, Benevento, Italy. [8]Present address: F.Hoffmann-La Roche AG, Basel, Switzerland. e-mail: velia.siciliano@iit.it

require the implementation of more genetic modules and thus additional cellular resources.

On the other end, small molecules employed ex-vivo induce a rapid and reversible response in treated cells[21,22]. Small molecules are widely used for several biological purposes, such as fine-tune protein expression[23,24], stem cell differentiation[25,26], immune cells expansion for bio-manufacturing of immunotherapies[22]. Their identification typically requires the screening of thousands of compounds, which is laborious and time consuming[27]. Recently, a computational tool named "*DECCODE*" (Drug Enhanced Cell COnversion using Differential Expression) was introduced to identify small molecules that were able to regulate cellular processes towards a targeted whole-genome transcriptomic signatures. DECCODE compares the expression profile of a target cellular state to those induced by a large collection of drug treatments, bypassing high-throughput screening for drug discovery. For each comparison, the method provides a similarity score measuring how much a given drug induces transcriptional features mimicking those observed in the target cells. Therefore, the approach is entirely data-driven and unbiased towards specific biological mechanism[28].

Prompted by the observation that certain genetic design can increase cell operation capacity, here we want to investigate whether similar effects could be achieved by drug treatment, providing an efficient and genetically non-invasive tool. Our hypothesis is grounded in the notion that small molecules influencing endogenous processes may shift the cells' internal resource distribution; in other words, when cells prioritize certain molecular activities in response to treatment, it reflects a reallocation of resources, even if the drugs were not originally designed with this effect in mind.

We thus sought to define the transcriptomic profile of H1299 cells expressing miRNA-iFFLs to interrogate the DECCODE algorithm for the identification of molecules that increase transgene expression rate of engineered cells (Fig. 1).

Next, the top compounds were tested in several experimental settings including protein production starting from DNA or RNA, viral production and transduction (Fig. 1). We also investigated whether the compounds may achieve the same effect in other cell types, demonstrating a host-dependent response analogous to genetic circuits designs. Collectively, our findings demonstrate that small molecules can be selected in a data-driven, mechanism-agnostic manner to enhance the productive capacity of engineered cells, with different applications in the bio-industrial fields. Although the compounds were prioritized based solely on their transcriptional similarity to iFFL-expressing cells, the resulting phenotypic effects suggest a convergent impact on mechanisms related to cellular resource allocation.

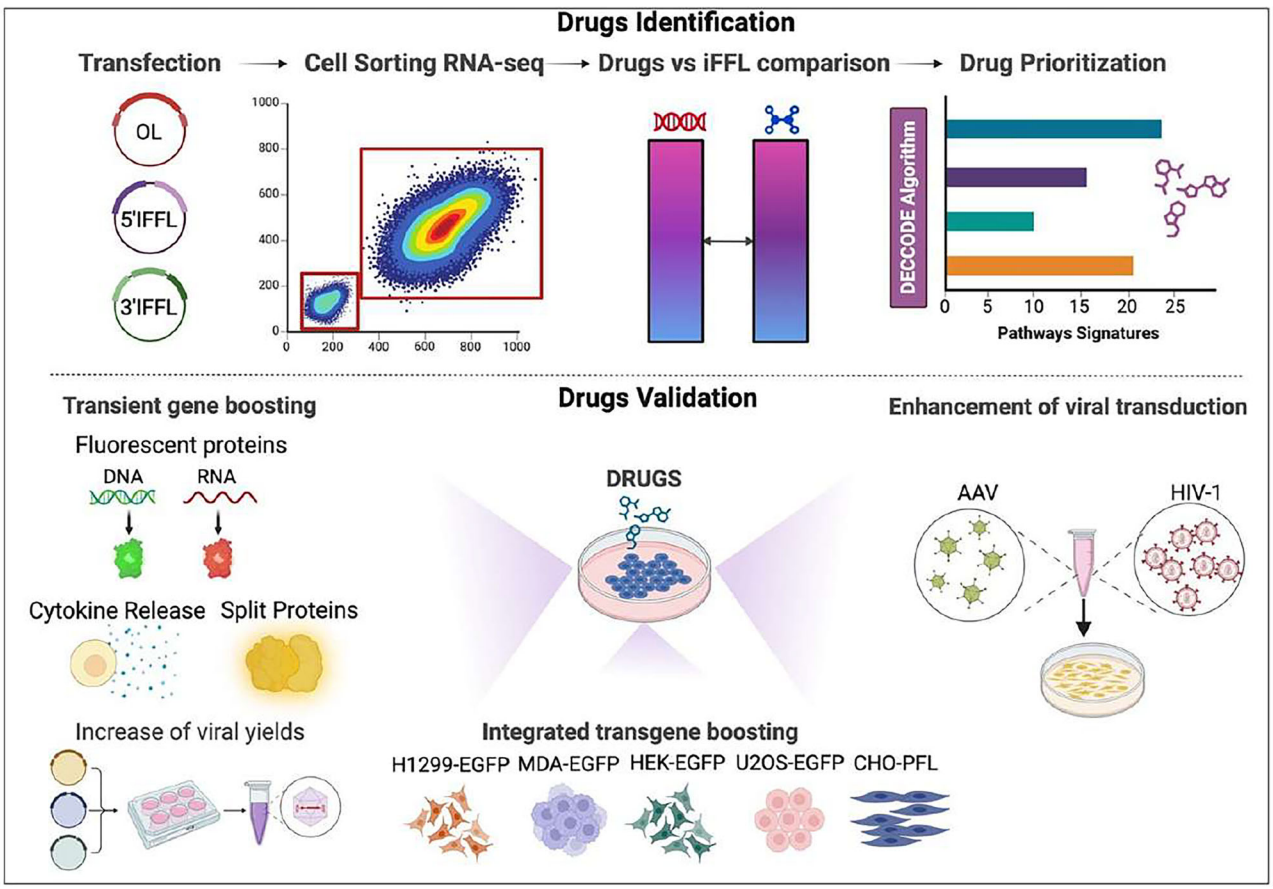

Fig. 1 | Pipeline of the study. *Top*: drug identification. H1299 cells transfected with EGFP and mKate fluorescent proteins in different circuit topologies, Open Loop (OL) and microRNA-Incoherent Feed-Forward Loop (miRNA-IFFL) were sorted according to fluorescence expression and RNA was extracted to carry out RNA-sequencing. A gene signature matrix was generated and converted into pathway signatures. Drug prioritization is obtained by DECODDE algorithm, comparing the transcriptomes of thousands of drug-treated cells with those generated by OL and miRNA-IFFL designs, to select drugs with profiles similar to those of miRNA-IFFLs. *Bottom*: drugs validation. Increased protein expression was evaluated and exploited in different experimental settings, including expression of genetic constructs encoded by DNA or RNA in transient (left), and integrated cell lines (middle). Finally, on a more applicative exploitation of DECCODE, we evaluated the effect of the leading drugs on viral transduction. *Created in BioRender. Siciliano, V. (2025)* https://BioRender.com/wyi8cf4.

Results

Identification of small molecules to increase the expression of exogenous genetic payloads by DECCODE

We have previously reported that cells have a finite amount of transcriptional and translational resources, resulting in a limiting productivity capacity[17,18]. We thus designed miRNA incoherent feed forward loop-iFFL[17] and observed upregulation of heterologous protein expression in the targeted cells upon a redistribution of cellular resources[20].

We then sought alternative means devoid of genetic footprints to increase cellular production of transgenes, based on cell treatment with small molecules identified by the computational tool DECCODE. To this end we first performed RNA-sequencing on H1299 cells, the testbed of our previous studies[17–20], co-transfected with a bi-directional plasmid encoding EGFP and mKate, either in an open loop circuit architecture (OL) that lack miRNA regulation, or as a miRNA-iFFL, by placing miR31-target sites, highly expressed in this cell line, in the 3′ (iFFL-3′) or 5′(iFFL-5′) UTR of mKate (Fig. 2a). We next sorted the cells that were either non-transfected (NTr) or transfected (Tr) according to fluorescence expression, to compare the OL, with iFFL-3′ and iFFL-5′ architectures that showed increased transgenes expression.

We performed Principal Component Analysis to investigate the distribution of NTr and Tr populations in a two-dimensional Cartesian space for the three transfection conditions (Supplementary Fig. 1). In the OL design, NTr and Tr populations are spatially separated (Supplementary Fig. 1a), while in the iFFL-3′ and iFFL-5′ configurations, the distance between populations progressively decreases (Supplementary Fig. 1b, c). We carried out the differential expression analysis on the three experimental groups to ensure that there would be distinct transcriptional signatures to feed DECCODE (Fig. 2b). As compared to iFFL samples, the OL exhibits the highest number of differentially expressed genes (Fig. 2b, *volcano plot, red circles*; Supplementary Table 1). Conversely the iFFL topology, especially when miR-31 target sites are located at the 5′UTR the system, shows reduced differential expression (Fig. 2b, *purple and green circles*). Next, we analyzed the biological pathways enriched based on the differentially expressed genes (FDR ≤ 0.1) across different transfection conditions. The number of dysregulated pathways is greater in OL samples (Supplementary Table 2), and several involve RNA processes, translation and post translational modification that are bottlenecks in protein production, indicating a correlation with resource distribution, as well as metabolism and energy production, crucial to cell fitness and activity (Fig. 2c). Other pathways relate to innate response to external nucleotides and viral particles (RIG-I signaling pathway), suggesting a possible limitation to the expression of exogenous payloads (Fig. 2c). Interestingly, RNA processing and translation pathways are still dysregulated in the 3′iFFL, but not in the 5′UTR, in agreement with the ribosome redistribution observed in our previous report[20], whereas pathways associated to innate immune response are still present in both 3′ and 5′ iFFLs.

Having confirmed the different transcriptional signatures in OL *versus* iFFL expressing cells, we next used DECCODE algorithm to identify small molecules that can increase gene expression of exogenous payloads. As required by the DECCODE approach, a single transcriptional model was obtained by comparing cells carrying the OL or the iFFLs (Fig. 2d). We merged all the profiles corresponding to cells with a significant transfection level, thus diluting the main source of variation in the data. The obtained differential profile was converted to a pathway expression profile based on the Gene Ontology—Biological Process collection. Of note, this analysis is substantially different from the previous (Fig. 2b, c), since it only considers the differences across the transfected conditions (OL, 3′iFFL, 5′iFFL), as compared to those intra-sample. Comparison against ~19,000 drug-induced pathway-based expression profiles from the Library of Integrated Network-Based Cellular Signatures (LINCS)[29] was performed to prioritize the corresponding molecules (Fig. 2d). Specifically, small molecules inducing a profile similar to those of miRNA-iFFL were ranked higher (Fig. 2e visualizes the top 30 hits based on pairwise structural distance). We performed a Drug-set Enrichment Analysis (DSEA)[30] of the top 30 ranked drugs to identify the common pathways on which the drugs have an impact and then compared them with the biological processes enriched in the RNA-seq data. Interestingly, several pathways related to RNA processes, protein translation and metabolism were affected by the drugs, suggesting a correlation with resources reallocation (Fig. 2f). Out of the top thirty we selected sixteen drugs based on commercial availability and tested their effects on fluorescent protein production in the OL configuration.

Selected small molecules increase expression of genes delivered as DNA or RNA in different cell lines

CMV-driven EGFP and mKate encoding plasmids were co-delivered in H1299 cells and treated with the selected compounds 4 h post-transfection. The timing was chosen based on plasmid uptake that occurs relatively early after transfection (within the first few hours)[31]. Four of the sixteen drugs, namely Ruxolitinib[32], TWS119[33], Filgotinib[34] and Tie2 kinase inhibitor 1 (TIE2)[35] which are FDA approved (Supplementary Note 1), increase fluorescence expression by ~10–50% compared to untreated cells (Fig. 3a, Supplementary Fig. 2). Ruxolitinib and TWS119 had the most significant response in this cell line, while Filgotinib exhibited high variability (Fig. 3a, Supplementary Fig. 3) with slightly increased mKate (~10%). To investigate whether the drugs effect depends on the amount of plasmid transfected, we assessed the cellular response to the compounds upon delivery of three different doses of plasmid DNA (60–180 ng/10^4 cells) (Supplementary Fig. 3). The results indicate that the effect of each drug is independent of the plasmid dose (Supplementary Fig. 3).

In a recent work, we optimized the simultaneous gene expression of EGFP and mKate by combining various genetic modules (promoter, Kozak, PolyA) in the plasmid designs[19]. This optimization was particularly effective when combining the HGHpolyA (CMV-EGFP-HGHpA) with the SV40polyA (CMV-mKate-SV40pA) in a 1:1 ratio in HEK293T. We confirmed that the same genetic combination improves the expression of both fluorescent proteins also in H1299 (Supplementary Fig. 4a). Notably, in the case of EGFP-HGHpA encoding plasmid, Filgotinib treatment resulted in higher protein production than untreated cells, in contrast to what observed with EGFP bearing the SV40polyA (CMV-EGFP-SV40pA) (Supplementary Fig. 4b) suggesting that combining genetic modules with drug treatment may enhance optimal gene expression. Furthermore, by steadily increasing the EGFP-HGHpA molar ratio, we found that this genetic design combination was also the least perturbing mKate expression, ensuring sustained levels of both genes across the different molar ratio, as compared to the EGFP-SV40polyA design (Supplementary Fig. 5).

Since we previously showed that exogenous payloads reduce overall cellular capacity[17–19] and that the mitigation by miRNA-iFFL[17,20] varies in a cell-dependent fashion, we evaluated whether the same genetic architecture could facilitate resource reallocation in additional cell lines, specifically U2OS, HeLa, and CHO-K1. To this end, we designed miRNA-iFFLs tailored to each line by incorporating target sites for miR-221 (U2OS) or miR-21 (HeLa and CHO-K1), based on their high endogenous expression in these cells[36–38]. Our data confirm that resource competition is consistent across cell types, and that the miRNA-iFFL design effectively redistributes resources to enhance transgene expression, in line with prior studies[17–19]. Notably, we also confirm that the impact of a given genetic design remains strongly cell-line dependent (Supplementary Fig. 6).

Building on this and considering our prior observations of pervasive cell-context effects on genetic part and circuit performance, we next asked whether the small molecules identified by DECCODE could similarly improve transgene expression in cell lines beyond H1299.

https://doi.org/10.1038/s41467-025-62529-9

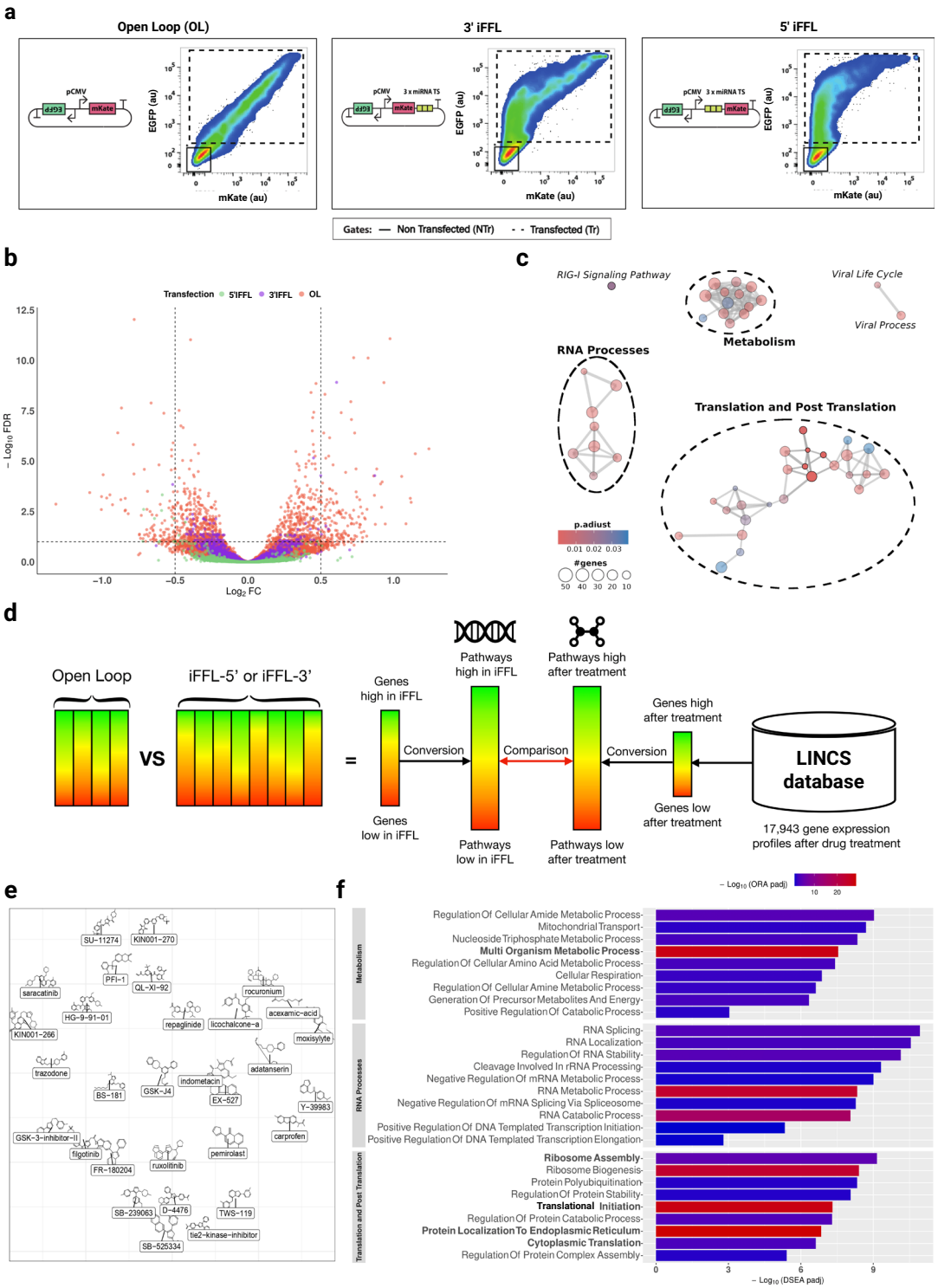

Fig. 2 | The transcriptomic landscape of burdened cells and drug identification by DECCODE. a Flow cytometry analysis of H1299 cells transfected with plasmids featuring three distinct circuit architectures: Open Loop (OL), 3′ miRNA-iFFL, and 5′ miRNA-iFFL. The 3′ and 5′ miRNA-iFFL include three target sites for miR31 which is expressed in the H1299 cell line. The dot plots illustrate the differing distributions of mKate fluorescent cell populations across the various circuit topologies. **b** Volcano plot depicting differential gene expression across the three circuits architecture, with the OL (red dots) showing the highest number and broadest range of DEGs. **c** Network visualization of significantly dysregulated pathway in cells transfected with the OL, including RNA processes, metabolism, translation and post-translation modifications. **d** Schematic workflow of DECCODE. The algorithm first compares differentially expressed genes in OL and iFFL transfected cells, identifying enriched pathways, which are then matched with drug-associated pathways using the LINCS database. **e** Visualization of the top 30 small molecules identified through DECCODE as selected by similarity to gene expression profiles observed in iFFLs. Spatial placement of the molecules is based on pairwise structural distance. **f** Common dysregulated pathways by Drug-set Enrichment Analysis (DSEA padj as bar length) of the top 30 drugs and by over-representation analysis (ORA padj as bar color) of cells transfected with the OL; pathways also enriched in iFFL designs are highlighted in bold.

https://doi.org/10.1038/s41467-025-62529-9

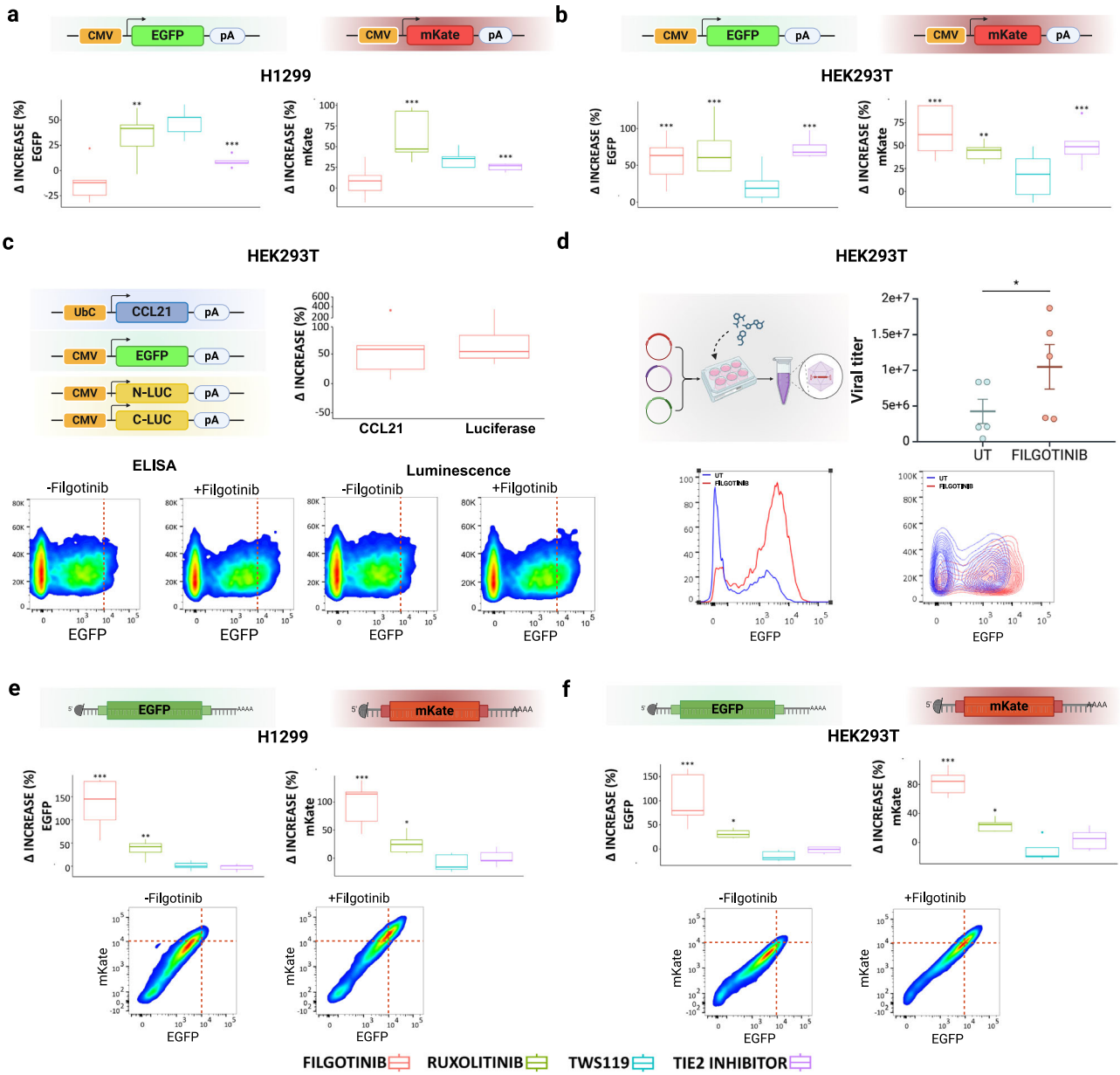

Fig. 3 | Effect of drug treatments on transient gene expression. a, **b** H1299 and HEK293T cells were transfected with plasmids encoding EGFP and mKate and then treated with the compounds. The boxplots illustrate the percentage increase of fluorescence intensity (drug color-code at the bottom of the panel). **c** Filgotinib treatment increased the release of the chemokine CCL21 and, in a split luciferase system, enhances Luciferase reconstitution and subsequent activity in HEK293T cells. The boxplot shows the percentage increase in CCL21 expression and luminescence following drug treatment. The density plots display EGFP fluorescence (co-expressed with CCL21 or with split-Luc) with and without Filgotinib treatment. **d** Filgotinib treatment during lentiviral production process significantly increases the lentiviral titer. The histogram and density plots illustrate the differences in number of transduced cells and fluorescence intensity w/wo Filgotinib. **e**, **f** RNA-encoded EGFP and mKate expression increases upon drug treatment, in particular with Filgotinib in H1299 and HEK293T cells. Transient transfection was performed with modRNAs. The density plots below illustrate the clear shift in fluorescence intensity with and without Filgotinib treatment. **d** Two-sided paired t-test for statistical analysis. Error bars represent standard error, SE. (**a**, **b**, **c**, **e**, **f**) Randomized block design ANOVA with Dunnett post hoc test for statistical analysis (*$p < 0.05$,**$p < 0.01$,***$p < 0.001$). $N = 5$ biological replicates. Boxplots indicate the median as the center line, the 25th and 75th percentiles as the bounds of the box, and the minimum and maximum values excluding outliers as the whiskers. Outliers are shown as individual points. Source data are included in the Source Data File. *Created in BioRender. Siciliano, V. (2025)* https://BioRender.com/c65c3eq.

We tested the effect of drugs treatment first in HEK293T and CHO-K1 cells, which are the workhorses of in vitro biological studies and bioproduction. Our results show that both EGFP and mKate protein levels increase by ~30–60% in HEK293T cells (Fig. 3b), whereas no significant differences were observed in CHO-K1 cells (Supplementary Fig. 7a). Overall, Filgotinib and Ruxolitinib were the most effective compounds, with Filgotinib, despite its milder effect in H1299 cells, emerging as the lead candidate in HEK293T cells.

We explored the effects of varying drug doses and treatment timings in HEK293T cells. The enhanced protein expression was maintained across most conditions, with the strongest effects observed when the drugs were administered 4–7 h post-transfection at concentrations of 10 or 15 μM (Supplementary Fig. 8).

To determine whether the increased gene expression induced by Filgotinib and Ruxolitinib leads to functional improvements, we evaluated outcomes such as protein secretion and circuit

performance in HEK293T cells, commonly used for genetic circuit prototyping and cell engineering. For secretion assays, we utilized the chemokine C-C motif ligand 21 (CCL21)[39], a cytokine involved in immunoregulation and inflammation, expressed under a UbC promoter. ELISA analysis revealed a 50% increase in CCL21 production following Filgotinib treatment (Fig. 3c). To assess circuit performance, a luciferase-encoding gene was split across two plasmids to form an AND gate-like system. Filgotinib treatment enhanced reconstitution efficiency, resulting in a 50% increase in luminescence (Fig. 3c). In both assays, an EGFP-expressing plasmid was co-transfected as a reference (Fig. 3c, *bottom*). Conversely, Ruxolitinib did not show improvements in these settings despite increasing EGFP expression (Supplementary Fig. 9). Since Filgotinib showed the most consistent effect in HEK293T cells, we sought to investigate whether lentivirus production, widely used to engineer different cell lines could benefit from the treatment. Lentiviral vectors are produced by transient expression of transfer and accessory plasmids in HEK293T cells. However, even if they can embed quite large genetic payloads, the efficiency of the production is inversely proportional to the size of the DNA fragments, a limitation for the engineering of genetic designs with multiple transcriptional units.

We co-transfected HEK293T cells with a lentiviral vector expressing EGFP under the control of a UbC promoter and accessory plasmids following well established protocols[40]. We then added the drugs 4 h post-transfection and collected the virus 72 h later, setting a control sample without drugs. Upon virus collection, we transduced HEK293T cells, and calculated the titer based on the population of EGFP-positive cells ("Material and Methods"). The results show that the treatment with Filgotinib increased the vector yield of 60% as compared to the untreated ones (UT) (Fig. 3d).

Lastly, as RNA-encoded circuits have emerged as a novel gene regulatory modality that addresses limitations of insertional mutagenesis and immunogenicity[41,42], we investigated whether drug treatment would benefit their expression. We co-transfected modified RNAs (modRNA) expressing EGFP and mKate and measured protein expression via flow cytometry 24 h post-delivery. Both H1299 and HEK293T cells remarkably increase EGFP and mKate expression by 100% with Filgotinib (Fig. 3e, f). Interestingly, CHO-K1 cells also exhibited higher protein expression from RNA-encoded circuits when treated with Filgotinib and Ruxolitinib (Supplementary Fig. 7b), suggesting that these drugs may influence post-transcriptional processes.

Overall, our findings indicate that Filgotinib and Ruxolitinib significantly boost gene expression and protein production across various experimental setups by DNA- or RNA-encoded genetic circuits.

Impact of small molecules on cell engineered by stable integration of transgenes

While transient transfections are typically performed for rapid prototyping of genetic circuits, stable integrations are used in industrial and biomedical assets. Therefore, we investigated the response to drugs of stably integrated genes either in steady state conditions (Fig. 4a *top right*), or during perturbations by exogenous payloads provided on-demand (Fig. 4a *bottom right*).

We first engineered H1299, HEK293T, U2OS, and MDA-MB231 cell lines with a lentiviral vector encoding a UbC promoter driving the EGFP (Fig. 4a, Supplementary Fig. 10). We assessed the impact of drug treatment on integrated gene expression by adding the four compounds to cultured cells, followed by flow cytometry analysis. H1299-EGFP and HEK-EGFP cells increased EGFP expression by 10-70%, with Filgotinib inducing the highest upregulation (Fig. 4b), whereas U2OS-EGFP, and MDA-MB231-EGFP did not respond to the treatment (Supplementary Fig. 10). To account for genetic payload diversity, we also generated a HEK293T cell line expressing mCherry under a shEF1a promoter and observed a similar trend in drug responsiveness (Supplementary Fig. 11).

Since we have previously demonstrated that the bottleneck of cellular productivity are the limiting resources, affecting endogenous genes upon synthetic genes transfections[17], we next investigated whether integrated genes are also perturbed by transient expression of exogenous payloads and if so, whether the drugs could mitigate the effect. In fact, recent work has demonstrated decreased expression of integrated genes when perturbed with plasmids that include promoters of varying strengths[43]. While those studies focused on landing pad integrated genes, typically featuring a single locus integration, we evaluated the effect upon lentiviral transduction, commonly used in various applications including cell-based therapies, which often require multiple copies of the integrated gene.

We carried out tests in H1299-EGFP, U2OS-EGFP, HEK-EGFP and MDA-MB-231-EGFP. Similar to what was observed in transient settings[12–14], also integrated genes undergo genetic perturbation in a cell line-dependent fashion. In H1299-EGFP and U2OS-EGFP cells, transfection with a CMV-mKate plasmid led to a 20–45% decrease in green fluorescence (Fig. 4c, *green boxplot*). In contrast, HEK-EGFP showed only a modest reduction (-10%) (Fig. 4c, *bottom, green boxplot*), and MDA-MB-231-EGFP displayed no change in protein expression (Supplementary Fig. 12). Beyond simple promoter–reporter constructs, we also investigated the positive feedback loop (PFL), a more complex regulatory architecture common in gene networks. To this end, we used CHO TET-OFF cells stably expressing the tetracycline-controlled transactivator (tTA), further engineered with a CMV-TET promoter driving expression of a tTA–d2EYFP fusion (CHO-PFL)[44,45]. In previous work, we characterized this circuit and compared it to a version lacking the feedback loop[44,45]. CHO-PFL cells exhibited limited upregulation of d2EYFP in response to Filgotinib and Ruxolitinib (Supplementary Fig. 13) but were strongly affected by CMV-mKate transfection (Fig. 4c, *green boxplot*). Finally, we tested whether Filgotinib, that induced the strongest upregulation of integrated genes, could also buffer against the effects of exogenous perturbation. In H1299-EGFP, HEK-EGFP, CHO-PFL, and U2OS-EGFP cells, Filgotinib treatment consistently reduced the impact of CMV-mKate transfection (Fig. 4c, *blue boxplot*). This protective effect may stem from enhanced overall protein expression promoted by Filgotinib, as mKate levels remained stable or slightly increased in treated samples (Supplementary Fig. 14).

Improving viral vector transduction by Filgotinib supplementation

We have previously shown that Filgotinib supplementation during lentivirus production increases the titer. Lentiviruses are broadly used in biotechnological industry and biomedical sector for the ability to easily integrate genetic payloads, as well as for the engineering of market-approved *living drugs* for the treatment of monogenic diseases and hematological malignancies[46].

However, transduction efficiency is hampered when lentiviruses include big genetic payloads, a limitation for complex regulatory network characterization in vitro. Also AAVs are largely used for basic science (i.e., to deliver genes into neurons to study neural circuits and brain-behavior relationships) and in vivo therapy. They can be engineered with tissue-specific tropism[47] and ensure long-lasting transgene expression, making them suitable as delivery tool for therapeutic genes in several genetic disorders. However, a major limitation is that depending on the serotype, transduction of cells ex vivo may be inefficient, making circuits prototyping in vitro prior in vivo experiments largely ineffective.

We investigated whether Filgotinib would improve lentivirus and AAV transduction in vitro, since it demonstrated the most consistent effect across the different experimental settings.

HEK293T cells were transduced with a lentivirus carrying a Ubc-EGFP and added the small molecule after 4 h (Fig. 5a). 72 h post-Filgotinib treatment we observed ~30% increase of EGFP-transduced

https://doi.org/10.1038/s41467-025-62529-9

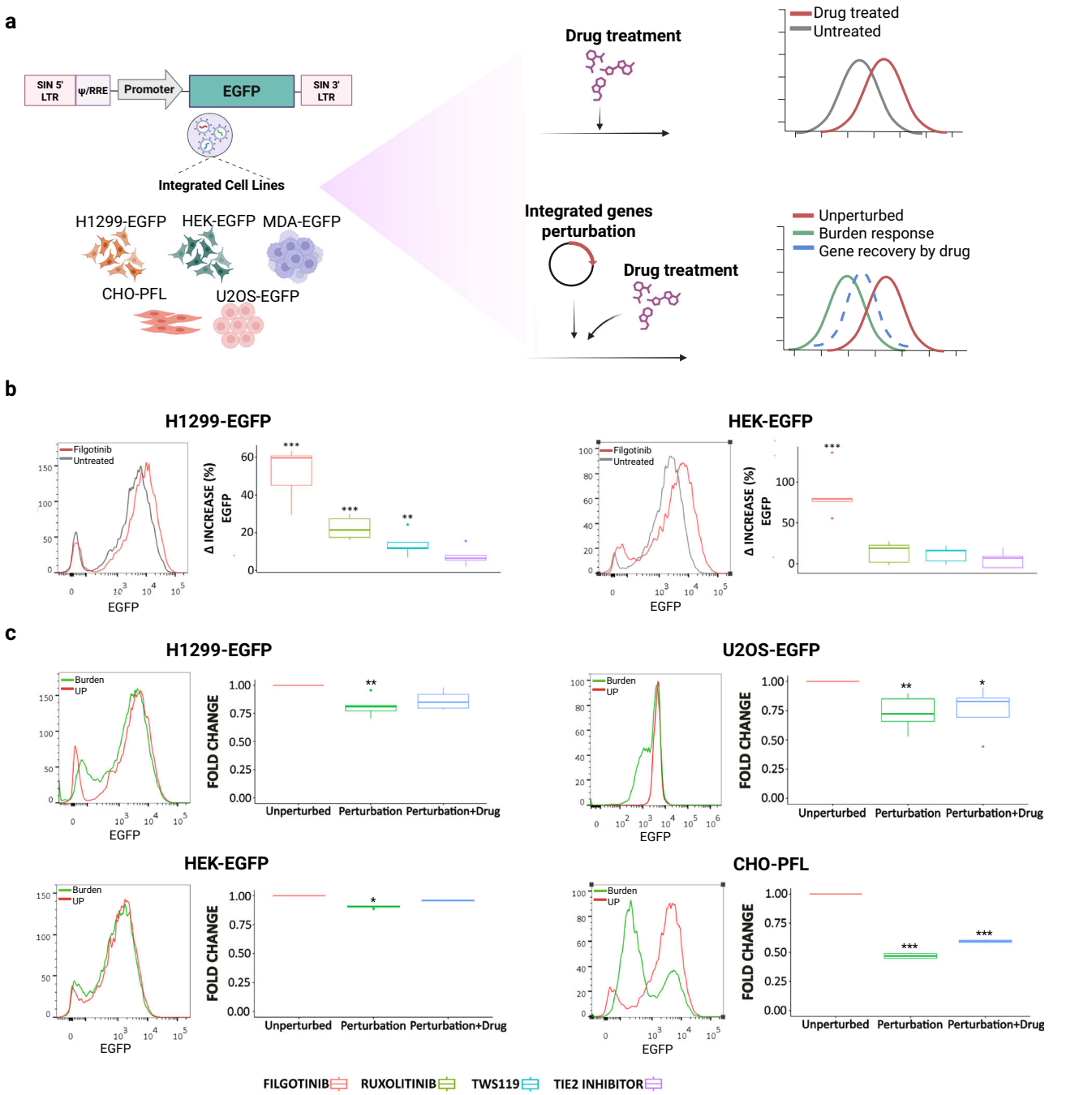

Fig. 4 | Effects of drugs treatment and transient perturbations on stably integrated genes in different cell lines. a Schematic representation of the experimental design. Cell lines H1299-EGFP, HEK-EGFP, MDA-MB231-EGFP, CHO-PFL, and U2OS-EGFP were generated by lentiviral transduction of a constitutive promoter driving EGFP. (*top right*) Cells were then treated with the compounds and changes in EGFP expression were analyzed by flow cytometry. (*bottom right*) Burden on integrated cells was applied by perturbation with a transiently transfected gene, and the response on EGFP expression and its recovery by the treatment with the drugs was evaluated by flow cytometry. **b** The four drugs increased expression of integrated payloads in H1299-EGFP and HEK-EGFP cell lines, in particular with Filgotinib. The histograms on the left compare EGFP expression levels in Filgotinib-treated versus untreated cells. The boxplots illustrate the percentage increase in EGFP expression following drug treatment. **c** Analysis of EGFP expression variations in H1299-EGFP, U2OS-EGFP, HEK-EGFP, and CHO-PFL cells under perturbation (green boxplot) and subsequent recovery by Filgotinib treatment (blue boxplot). Histograms depict EGFP expression profiles for cells unperturbed and on burden condition. Box plots illustrate the fold change in EGFP expression, highlighting the recovery effects of the various drugs. **b**, **c** Randomized block design ANOVA with Dunnett post hoc test for statistical analysis ($^{*}p < 0.05$,$^{**}p < 0.01$,$^{***}p < 0.001$). Boxplots indicate the median as the center line, the 25th and 75th percentiles as the bounds of the box, and the minimum and maximum values excluding outliers as the whiskers. Outliers are shown as individual points. **b** $N = 5$ biological replicates. **c** $N = 4$ biological replicates. Source data are included in the Source Data File. *Created in BioRender. Siciliano, V. (2025)* https://BioRender.com/t2mwxl7.

cells as compared to untreated samples (Fig. 5b, c). We next tested various lentiviral MOIs to assess the impact of Filgotinib treatment relative to viral concentration. We evaluated three different MOIs of the same lentiviral vector, and Filgotinib treatment consistently increased the percentage of transduced cells across all conditions (Fig. 5d). Notably, the effect was most pronounced at the lowest MOI (0.1), suggesting increased sensitivity to the compound under suboptimal transduction conditions (Fig. 5d).

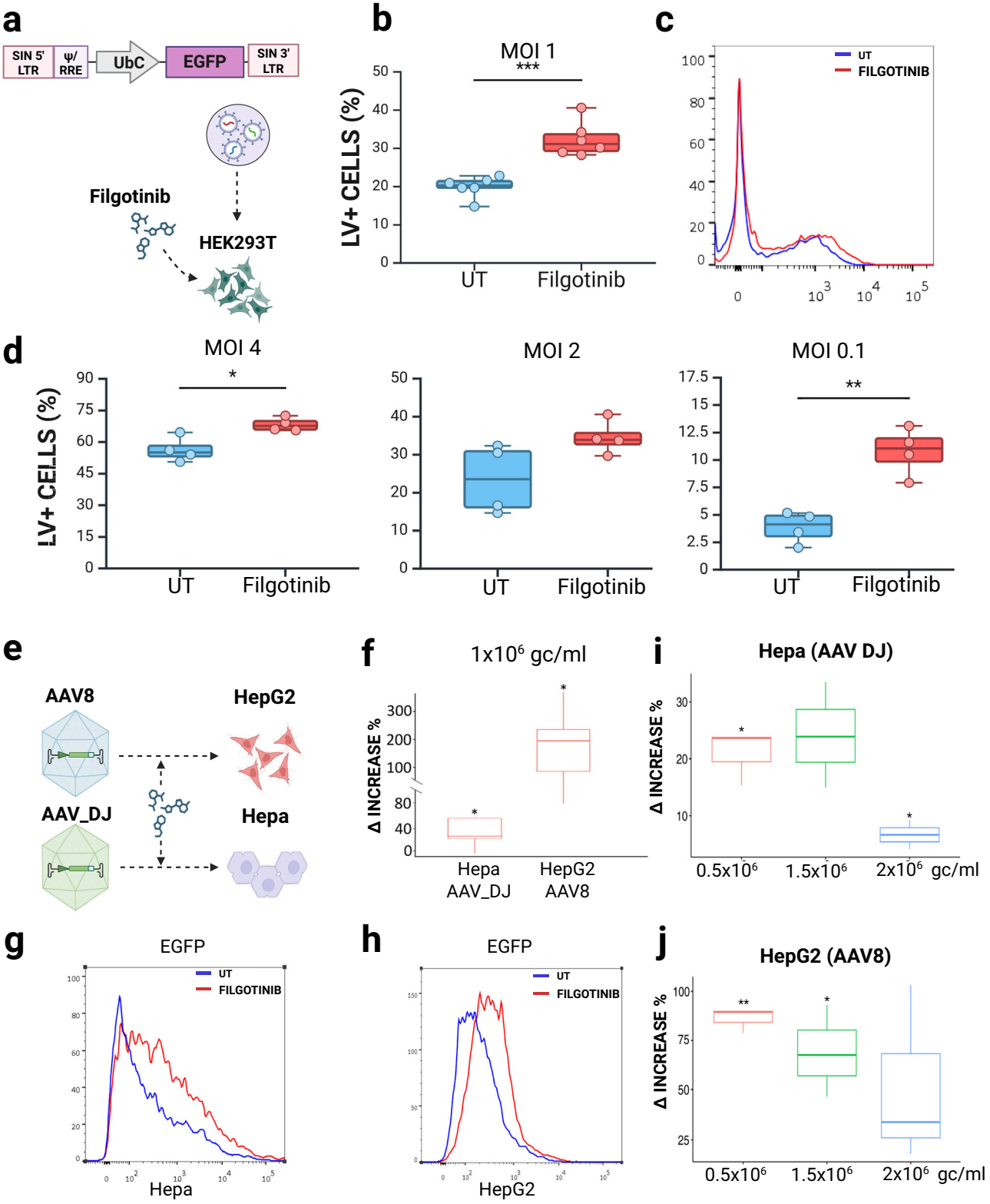

To assess whether Filgotinib improves AAV-mediated gene delivery, we used hepatotropic AAVs, namely AAV8 and AAV_DJ, and we transduced HepG2 and Hepa1-6 (Hepa) hepatocytes. AAV8 is a natural AAV, while AAV_DJ is a type 2/type 8/type 9 chimera, distinguished from its closest natural relative (AAV-2) by 60 amino acids in the capsid[48]. In specific, HepG2 were transduced with AAV8 serotype expressing EGFP fluorescence driven by a TGB promoter, whereas Hepa cells deriving from murine hepatoma and less prone to AVV8[49,50], were transduced with AAV_DJ that had already demonstrated to outperform standard AAV serotypes for in vitro transduction[48] (Fig. 5e). Hepa cells transduced with AAV_DJ exhibited a 40% increase of transduced cells, whereas HepG2 treated with Filgotinib upon AAV8 transduction exhibited 100% increase of EGFP+ cells (Fig. 5f). We then evaluated three different MOIs of AAV_8 and AAV_DJ vectors, followed by Filgotinib treatment, and found improved transduction efficiency in all cases (Fig. 5i, j), with the greatest enhancement observed at the

Fig. 5 | Enhancement of viral transduction by Filgotinib treatment. a Schematics of Filgotinib treatment during lentiviral transduction to improve efficiency in HEK293T cells. **b** Percentage of transduced cells in untreated and Filgotinib samples (MOI = 1). **c** Exemplative histogram of lentiviral transduced cells w/wo Filgotinib. **d** HEK293T cells transduced with different MOI of lentivirus and treated with Filgotinib. Boxplots represent the percentage of positive cells in the untreated (UT) sample and Filgotinib samples. **e** Schematics of AAV transduction followed by Filgotinib treatment in hepatocyte-like cell lines Hepa and HepG2. **f** Percentage increase of AAV-positive cells after transduction and Filgotinib supplementation (**g**, **h**) Exemplative histograms displaying the differences in AAV expression in Hepa and HepG2 w/wo Filgotinib. (i-j) Hepa and HepG2cells were transduced with varying MOI of AAV_DJ and AAV8, respectively, and treated with Filgotinib. Boxplots represent the Δ increase (expressed in percentage) of the AAV positive cells comparing Filgotinib and UT samples. (**b**, **d**, **f**) Two-sided paired *T*-test for statistical analysis (*$p < 0.05$,**$p < 0.01$,***$p < 0.001$) or (**i**, **j**) Two-sided paired *t*-test with the *p* values were adjusted for multiple comparisons using the FDR method. (*padj < 0.05,**padj < 0.01).; (**b**, **d**, **h**, **i**) $N = 3$ biological replicates. **b**–**f**$N = 4$ biological replicates. Boxplots indicate the median as the center line, the 25th and 75th percentiles as the bounds of the box, and the minimum and maximum values excluding outliers as the whiskers. Outliers are shown as individual points. Source data are included in the Source Data File. *Created in BioRender. Siciliano, V. (2025)* https://BioRender.com/8ybz63h.

lowest MOI tested (0.5×10^6 gc/ml). These results support the potential utility of small-molecule treatment in conditions where gene expression is not yet saturated.

Last, we investigated the effect of Filgotinib supplementation on a population of HepG2 cells transduced by AAV_DJ (transduction efficiency close to 100%) and observed an increase of EGFP fluorescence of transduced cells as compared to the untreated cells (Supplementary Fig. 15). Collectively these data indicate that Filgotinib can be effectively used in a variety of applications for virus-delivered genetic design screenings and prototyping.

Transcriptional landscape of Filgotinib treated cells

We performed RNA-sequencing on H1299, HEK293T transfected with plasmids expressing EGFP and mKate in an open OL, w/wo compound supplementation, or with iFFL circuit, to have insights on molecular changes occurring upon Filgotinib treatment (Supplementary Note 1). Notably, pathways related to RNA processing were found to be commonly affected by both the iFFL topology and Filgotinib treatment, suggesting that post-transcriptional, translational and post-translational processes may be a key target of the drug (Supplementary Figs. 16, 17, 19).

Conversely, most housekeeping genes, with different functions in the cell, were stable in Filgotinib-treated cells, suggesting that it does not impair essential cellular functions (Supplementary Fig. 20). Since CHO-K1 cells did not respond to Filgotinib upon DNA plasmid transfection, we carried out RNA-seq also in this cell line. In agreement with the flow cytometry data, we did not observe relevant differences at the transcriptomic level (Supplementary Fig. 17). We found interesting that CHO-K1 cells did not respond to Filgotinib upon DNA transfection, while enhancing protein production after RNA delivery. Our hypothesis is that CHO-K1 cells resilience to drug treatment when transfected with DNA is due to the efficient transcriptional machinery that compensates for translational bottlenecks. It was reported in Malm et al. that, as compared to HEK293 cells, genes associated to translation are less expressed in CHO cells[51]. We confirm in our RNA-seq data that the fraction of genes associated to translation is lower in CHO-K1 (Supplementary Fig. 18). This is in line with enhanced protein production that we observed upon RNA transfection (where the transcriptional component is missing) in cells treated with Filgotinib. Further supporting this notion, we observed that different combinations of polyA signals, which influence post-transcriptional regulation, exhibited diverse effects in CHO-K1 cells compared to HEK293T line[19]. This reinforces the idea that CHO-K1 cells differ in how they utilize transcriptional and translational resources.

We then compared the pathways resulted from RNA-seq data and previously obtained DSEA on the top four drugs (Fig. 2f), and we found an enrichment of pathways that relate to RNA stability and maturation, ribosome assembly, and tRNA metabolism, supporting the hypothesis of a general impact on the post-transcriptional processes and translation especially in H1299 and HEK293T (Supplementary Fig. 21). Conversely, no pathway seems to be involved in CHO-K1 cells as expected from previous analysis. Filgotinib is a known inhibitor of the JAK-STAT pathway specifically targeting JAK1 to block STAT activation and reduce pro-inflammatory cytokine signaling[52,53](Supplementary Note 1). Given its known mechanism, we investigated whether the observed enhancement of cellular productivity could be attributed to JAK1 inhibition. To test this, we silenced JAK1 in the H1299-EGFP cell line using JAK1-specific siRNA and measured EGFP expression to mimic the conditions of Fig. 4b. Despite effective JAK1 knockdown, EGFP expression did not recapitulate the increase seen with Filgotinib treatment (Supplementary Fig. 22, *left*), suggesting that JAK1 inhibition alone is insufficient to explain the drug's effect. Interestingly, Filgotinib treatment led to an upregulation of JAK1 transcript levels (Supplementary Fig. 22, *right*), consistent with a broader enhancement of gene expression reminiscent of miRNA-based iFFL effects[20]. To further investigate, we profiled the expression of genes involved in the JAK-STAT pathway (as annotated in the KEGG database) in HEK293T and H1299 cells with and without Filgotinib treatment. The expression patterns differed notably between the two lines (Supplementary Fig. 23). In HEK293T cells, which respond robustly to Filgotinib, we observed upregulation of STAT1, STAT3, IRF9, and the IL2α receptor, while IL4 and EGFR receptors were downregulated. Conversely, in H1299 cells, STAT1, STAT3, IRF9, IL2α, and IFN1α receptors were downregulated. The only shared changes were reduced expression of IL4 and erythropoietin receptors. Given these divergent responses, it is unlikely that JAK-STAT signaling is the principal pathway mediating Filgotinib's enhancement of gene expression.

This interpretation is further supported by the nature of our experimental system, which does not involve immune cells—the primary context in which JAK/STAT signaling plays a central functional role. Our experimental settings is quite different from the in vitro studies on the drug carried out on peripheral blood mononuclear cells and whole blood from healthy volunteers and patients with rheumatoid arthritis (RA)[54]. It should be also considered that previous studies on Filgotinib were related to its role for the treatment of RA, therefore other potential effects are not known. Therefore, we believe that Filgotinib's productivity enhancing effects occur independently of JAK/STAT-driven mechanisms.

Discussion

This study lays the groundwork of deploying computational algorithms for the identification and selection of small molecules that can enhance exogenous gene expression, advancing industrial biomanufacturing and gene therapy vector prototyping. Limited cellular resources is a pervasive issue that affects the engineering of multiple organisms ranging from bacteria[55,56] to mammalian cells[17,18]. Over the past few years, various strategies including genetic modules and alternative regulatory architectures have been proposed to increase cells operational capabilities[17–19]. By combining computational tools and experimental designs, we here provide an approach to increase cell productivity, which neglects both the modular composition of gene expression cassettes, and the network architecture. Small molecules can regulate several processes in the cells, including the production efficiency of exogenous DNA and RNA material. Through DECCODE algorithm[28], we

have identified compounds that upregulate protein expression with no prior information about the mode of action, avoiding biases on the bottlenecks of intracellular resources. Of the top sixteen drugs selected by DECCODE, Ruxolitinib, TWS119, Filgotinib and TIE2 inhibitor were exhibiting an enhancing effect on protein production and Filgotinib had consistent responses in a variety of different settings. While DECCODE performed computation on transcriptional data collected for H1299 cells, we explored the potential applications to other cell lines. Notably, analogously to gene expression modules, the effect of the drugs, is cell context dependent.

The highest increase of transgene expression was achieved with Filgotinib and Ruxolitinib, the first emerging as lead candidate across several settings. The effect of Filgotinib on viral preparation and transduction can significantly improve the scalability and efficiency of vector screening and production, holding promising applications in biomanufacturing and gene therapy prototyping. For instance, the viral production costs can be drastically reduced by increasing the titer with compound supplementation. Interestingly, we also observe that the Filgotinib treatment can support the optimization of gene expression of previously characterized genetic regulatory elements (e.g., HGHpolyA) (Supplementary Fig. 5), opening further horizons of synergistic combinations to tune gene expression in a desired manner, facilitating applications across a broader spectrum of cell types and genetic constructs.

A limitation of our study is that we did not investigate the molecular mechanisms underlying the effects of the small molecules, focusing instead on the phenotypic outcomes. However, we performed RNA-sequencing analysis upon Filgotinib treatment in HEK293T and H1299 cells, to capture transcriptomic changes, providing initial insights that can inform future mechanistic studies (Supplementary Note 2). Overall, our results suggest that both cell lines exhibit changes in pathways linked to protein production, including RNA processing, translation, and metabolism. These findings suggest that Filgotinib's ability to modulate such pathways may underline the observed enhancement in gene expression. In addition, in H1299 cells,also pathways related to stress response and innate immunity were enriched (Supplementary Note 2). The transcriptomic data generated here provide a valuable foundation for future mechanistic studies into the molecular functions of Filgotinib.

In summary, our study demonstrates the power of combining computational algorithms with synthetic devices to increase cellular productivity without needing detailed prior knowledge of drug mechanisms or resource competition bottlenecks. This approach has significant potential for in vitro systems and could pave the way for more efficient biomanufacturing and rapid prototyping of genetic circuits for therapeutic applications.

Materials and methods

Cell culture

HEK293T, U2OS, MDA-MB231, HeLa and Hepa cells used in this study were cultured in Dulbecco's modified Eagle medium (DMEM, Gibco); H1299 were cultured in Roswell Park Memorial Institute medium (RPMI, Gibco); CHO-K1 were cultured in α-MEM (Sigma Aldrich, M4526); HepG2 were maintained in MEM-E. All cell lines are from ATCC.

All media were supplemented with 10% FBS (Atlanta BIO), 1% penicillin/streptomycin/L-Glutamine (Sigma-Aldrich) and 1% non-essential amino acids (HyClone).

The cells were maintained at 37 °C and 5% CO2.

Stable cell lines engineering

H1299-EGFP, HEK-EGFP, MDA-MB231-EGFP and U2OS-EGFP were generated by transduction with a lentivirus carrying an EGFP gene under the UbC promoter. HEK-mCherry were obtained by transducing cells with a lentivirus carrying a shEF1α-mCherry construct. In all the cases 8×10^5 cells were plated in a 6 multiwell, and the virus was added in a ratio 1:3 with the culture medium 6 h after the plating. Cells were analyzed 1 week after transduction to assess the fluorescence and then maintained and amplified as described previously.

CHO-TET-OFF cells (Clontech #630904) transduced with a lentivirus containing CMV-TET promoter that drives the expression of tTA and d2EYFP described in Siciliano et al. paper[27] were a kind gift from Diego di Bernardo (Telethon Institute of Genetics and Medicine-TIGEM, Naples, Italy).

Transfections

Transfections were carried out in 24-well plate for flow cytometry analysis.

H1299 cells were transfected with Lipofectamine® 3000 according to manufacturer's instructions using 300 ng of total DNA in 24-well plates. CHO-K1 and HEK293T were transfected with PEI MAX® (POLYSCIENCES EUROPE gmbh) transfection reagent with 300 ng of total DNA in 24-well plates. 70000 to 80000 cells per well were plated ~24 h before transfection. At the moment of transfection, cells were put in starvation conditions for the first 24 h. DNA was diluted in Opti-MEM reduced serum media (Gibco), before being mixed and incubated for 25 min prior to addition to the cells. All drugs were added 4 h after transfection. Total of 80 ng of modified-RNAs (modRNA) were transfected using Lipofectamine® 3000 protocol under modified conditions in which no P3000 reagent was used. RNA was first diluted in Opti-MEM reduced serum media (Gibco) and it was then mixed with diluted Lipofectamine reagent as per manufacturer's instructions. The mix was incubated for 7 min prior to addition to the cells. The fast-forward protocol was used by seeding 120,000 cells per well in 24-wells plates at the moment of transfection.

DNA cloning and plasmids constructions

Plasmid vectors carrying gene cassettes were created using In-Fusion HD cloning kit (Clonetch), Gibson Assembly, via digestion and ligation or using the EMMA toolkit[57].

For plasmids with miRNA TS, the target sequences were selected using miRBase database (http://www.mirbase.org) and cloned into plasmids with the OligoAnnealing technique.

All plasmids were confirmed by sequencing analysis. All plasmids are listed in Supplementary Table 3.

modRNA production

Modified-RNAs were produced by in vitro transcription (IVT) performed using MegaScript T7 kit (Life Technologies). In the IVT reactions, modified conditions were used: GTPs were replaced by GTPs mixed with Anti Reverse Cap Analog (New England BioLabs) at the ratio of 1–4; while CTPs and UTPs were replaced by 5-methylcytosine-triphosphate and pseudouridine-triphosphate (TriLink BioTechnologies), respectively. Transcripts were then treated with Turbo DNase included in MegaScript T7 kit (Life Technologies) for 30 min at 37 °C and purified using MEGAclear™ Transcription Clean-Up Kit (Life Technologies). Lastly, resulting modified mRNAs (modRNAs) were incubated with Antarctic Phosphatase (New England BioLabs) for 30 min at 37 °C and purified again.

Drug preparation

All small molecules are commercially available and purchased by Selleck except for TWS119 that is from VWR. All compounds are dissolved in DMSO. Ruxolitinib and Filgotinib are used 10uM[32,34]. TWS119 is used 2uM[33] and TIE2 inhibitor is used 5uM[35]. For the dose response experiment drugs are also used at different concentrations.

Lentivirus production

Lentivirus productions were carried out in 6-well plate in HEK293T cells. HEK293T were transfected with second-generation

lentiviral plasmids with transfer vector and packaging plasmids in a ratio of 2:1:1 using the transfection method described above. Drugs were added 4 h after transfection. Media was changed 24 h after transfection with complete media and no drugs was added afterwards. The virus was collected 72 h after transfection and concentrated with Lenti Concentrator (OriGene technologies) following manufacturer instructions. Cell lines were transduced with same MOI.

Lentivirus and AAV transduction

Lentivirus and AAV transduction were carried out in 24-well plates.

Lentivirus was added to cells at MOI 1.

The AAVs were used at an MOI of $1 \times 10e^5$ gc/cell. The virus is added to incomplete media, incubated for 2 h and 30 min, and then added to plated cells. Drugs were added 4 h after AAV infection. For the experiment with diffent viral concentration the protocol of transduction is the same. The Lentivirus was added at MOI of 4; 2; 0,1. AAVs were used at MOI $0.5 \times 10e^5$ gc/cell; $1.5 \times 10e^5$ gc/cell and $2 \times 10e^5$ gc/cell.

Lentivirus titer

Lentivirus titrations were carried out in 24-well plates. Lentivirus was added to cells at the dilution of 1:50; 1:100; 1:200; 1:500.

After 72 h the EGFP fluorescence was measured by flow cytometry and based on the samples with a percentage of fluorescence of 20–40% titer was calculated with this formula:

$$T = \frac{N * F * D}{V_T}$$

where T = Titer, TU/mL; N = Number of cells transduced; F = Fraction of cells with fluorescence; D = Dilution Factor; V_T = Transduction Volume, ml[40].

AAV production

AAVs were provided by Nicola Brunetti Pierri (Telethon Institute of Genetics and Medicine-TIGEM, Naples, Italy) The pAAV2.TBG.GFP[58] was used for production of both AAV_Dj and AAV_8 serotype vectors. AAV vectors were produced by Innovavector s.r.l., Italy, by triple transfection in HEK293T cells; next were purified by CsCl2 ultracentrifugation and titered (in genome copies/milliliter) by real-time PCR and dot blot analysis.

Flow cytometry and data analysis

All cells were analyzed with a BD CELESTA™ cell analyzer (BD Biosciences). For each sample >10000 singlet events were collected. Cells transfected in 24-well plate were washed with DPBS, detached with 50 µl of Trypsin-EDTA (0.25%) and resuspended in 300 µl of FACS medium. Fluorescence intensity in arbitrary units (au) was used as a measure of protein expression. For each experiment a compensation matrix was created using unstained (wild type cells), and single-color controls (mKate only, EGFP only).

Population of live cells and single cells were selected according to FCS/SSC parameters. Data analysis was performed with FlowJo.

ELISA assay

ELISAs are performed with the Human Secondary Lymphoid-tissue Chemokine (CCL21) (SLC) Uncoated ELISA Kit (ThermoFisher Scientifics). Supernatant were harvested from 24 well plates with transfected H1299 or HEK293T cells 48 h after transfection and CCL21 was quantified according to manufacturer instructions.

Luminescence assay

Luminescence assays were performed on transfected HEK293T cells 48 h after transfection with split luciferase to detect luciferase activity. The luciferase activity was performed by Steady-Glo Luciferase Assay System (Promega). A volume of SteadyGlo reagent was added to 100 µl of cultured cells in a white 96 multiwell plate, following the manufacturer instructions 5 min after the addiction of the reagent we measured the luminescence on Glomax multimode microplate reader and normalized by the number of cells counted prior to the assay.

RNA-seq samples preparation

For the first RNA-seq analysis Qiagen RNeasy mini plus Kit (Qiagen) was used for RNA isolation. 10 µL of RNA at the exact concentration of 50 ng*µL −1 were provided for library preparation to the NGS facility of the Telethon Institute for Genetis and Medicine-TIGEM (Naples, Italy). Libraries were prepared using QuantSeq 3′ mRNA sequencing for RNA quantification kit (Lexogen). Samples were processed with NovaSeq 6000 System (Illumina).

For the second RNA-seq analysis Ethanol/Chloroform method combined with Zymo Clean&Concentrator Kit was used for RNA isolation. 10 µL of RNA at different concentration with a minimum quantity of 400 ng were provided for library preparation to the IIT facility. Library have been prepared with a TruSeq Total RNA seq with Ribo 0 Plus protocol and sequenced on NovaSeq 6000 in paired-end 2×100 bp. 44×106 raw reads/sample have been obtained in mean.

Quality parameters confirmed the high quality of sequencing data. After pre-processing steps for the removal of low-quality reads, reads have been aligned on the human genome assembly GRCh38—hg38. Samples were processed with NovaSeq 6000 System (Illumina).

RNA-Seq analysis

Sequence reads were trimmed using bbduk software (https://www.lexogen.com/quantseqdata-analysis/) to remove adapter sequences, poly-A tails and low-quality end bases. Alignment was performed with STAR[59] on the Homo sapiens reference (hg38) provided by UCSC Genome Browser. The expression level of genes was determined with htseq-count[60] using the Gencode/Ensembl gene model. Differential expression analysis was performed using DESeq2[61], a statistical package based on a model using the negative binomial distribution. Only genes with FDR 0.1 were considered differentially expressed for each comparison and were used to determine whether known biological functions or processes are enriched by clusterProfiler package[62].

DECCODE analysis

The Gep2Pep R/Bioconductor package[63] was employed to obtain the pathway-based expression profiles of the using 14,645 gene sets from 16 different gene set collections included in the MsigDB v6.1[64]. This version was chosen to match the precomputed pathway-based version of the LINCS drug-induced profiles dataset that is publicly available[63]. As previously described[27], the gene set database retaining most of the gene-based information (i.e., "Gene Ontology - Biological Process") was selected for further analysis. Finally, the DECCODE method was applied to prioritize pathway based LINCS[29] profiles based on their similarity to the target signature. The similarity scores were obtained as the reciprocal of the Manhattan distance between each profile pair after ranking pathways by their Enrichment Scores.

Statistics and reproducibility

Each experiment was repeated independently at least three times with similar results. To compare multiple drugs, statistical analysis was performed using a randomized block design ANOVA with two additive factors: treatment and experiment. The treatment factor, which was the factor of interest, consisted of the different drugs used to treat the cells. The experiment factor, known as the block, was used to control a known source of variability and its levels were constituted by the different experiments. This was followed by a Dunnett post hoc test to identify significant differences among groups. For comparisons between two conditions, a two-tailed paired *t*-test was used. Both ANOVA and *t*-test were performed on the log-transformed data. In the

figures, we represent the percentage increase, or the fold change calculated on the log-transformed data, comparing the drug treated with the untreated sample. To calculate the percentage increase, we used the formula:

$$\left[\frac{(D-C)}{C}\right] * 100$$

To calculate the fold change, we used the formula:

$$\frac{D}{C}$$

In both cases D is the Drug treated sample and C is the control (untreated sample).

The threshold for significance was set to 0.05 for the global ANOVA and *t*-test *p* values, as well as for the adjusted *p* values in the post hoc analysis. Prior to any testing, we assessed the normality of the data using the Shapiro-Wilk test and checked for homogeneity of variance using the Levene's test.

Reporting summary

Further information on research design is available in the Nature Portfolio Reporting Summary linked to this article.

Data availability

All relevant data are included as Source Data and/or are available from the corresponding author on reasonable request. Plasmids used in this study are available from the corresponding author on reasonable request. The RNA-sequencing data generated in this study have been deposited to ArrayExpress under accession code E-MTAB-14355 and E-MTAB-15146. Source data are provided with this paper.

References

1. Clubb, J. D., Gao, T. A. & Chen, Y. Y. Synthetic biology in the engineering of CAR-T and CAR-NK cell therapies: facts and hopes. *Clin. Cancer Res.* **29**, 1390–1402 (2023).
2. Bonfá, G., Blazquez-Roman, J., Tarnai, R. & Siciliano, V. Precision tools in immuno-oncology: synthetic gene circuits for cancer immunotherapy. *Vaccines* **8**, 1–17 (2020).
3. Caliendo, F., Dukhinova, M. & Siciliano, V. Engineered cell-based therapeutics: synthetic biology meets immunology. *Front. Bioeng. Biotechnol.* **7**, 1–8 (2019).
4. Astin, A. Engineering outcomes. *AW Astin ASEE Prism* **3**, 27–30 (1993).
5. Postiglione, L. et al. Regulation of gene expression and signaling pathway activity in mammalian cells by automated microfluidics feedback control. *ACS Synth. Biol.* **7**, 2558–2565 (2018).
6. Farquhar, K. S. et al. Role of network-mediated stochasticity in mammalian drug resistance. *Nat. Commun. 2019 101* **10**, 1–14 (2019).
7. Gutiérrez-Granados, S., Cervera, L., Kamen, A. A. & Gòdia, F. Advancements in mammalian cell transient gene expression (TGE) technology for accelerated production of biologics. *Crit. Rev. Biotechnol.* **38**, 918–940 (2018).
8. Cella, F. & Siciliano, V. Protein-based parts and devices that respond to intracellular and extracellular signals in mammalian cells. *Curr. Opin. Chem. Biol.* **52**, 47–53 (2019).
9. Bonfá, G., Cella, F. & Siciliano, V. Engineering protein-based parts for genetic devices in mammalian cells. *Methods Mol Biol.* **2229**, 331–346 (2021).
10. O'Flaherty, R. et al. Mammalian cell culture for production of recombinant proteins: a review of the critical steps in their biomanufacturing. *Biotechnol. Adv.* **43**, 107552 (2020).
11. Russo, L., De Martino, I., Marchetti, M. & Siciliano, V. Engineered T cells and macrophages: two arms to seize solid tumors. *Curr. Opin. Biotechnol.* **93**, 103296 (2025).
12. Blazquez-Roman, J., Pisani, M. & Siciliano, V. Engineering cell-based therapies. 271–285. https://doi.org/10.1016/B978-0-12-824469-2.00023-3 (2022).
13. di Bernardo, D., Marucci, L., Menolascina, F. & Siciliano, V. Predicting synthetic gene networks. *Methods Mol. Biol.* **813**, 57–81 (2012).
14. Cella, F., Martino, I. De, Piro, F. & Siciliano, V. Engineering programmable RNA synthetic circuits in mammalian cells. *Curr. Opin. Syst. Biol.* **28**, 100395 (2021).
15. MacDonald, J. T. & Siciliano, V. Computational sequence design with R2oDNA designer. *Methods Mol. Biol.* **1651**, 249–262 (2017).
16. Stone, A., Youssef, A., Rijal, S., Zhang, R. & Tian, X. J. Context-dependent redesign of robust synthetic gene circuits. *Trends Biotechnol.* **xx**, 1–15 (2024).
17. Frei, T. et al. Characterization, modelling and mitigation of gene expression burden in mammalian cells. *Nat. Commun.* 867549. https://doi.org/10.1101/867549 (2020).
18. Jones, R. D. et al. An endoribonuclease-based feedforward controller for decoupling resource-limited genetic modules in mammalian cells. *Nat. Commun.* **11**, 1–16 (2020).
19. Di Blasi, R. et al. Resource-aware construct design in mammalian cells. *Nat. Commun.* **14**, 1–10 (2023).
20. Cella, F. et al. MIRELLA: a mathematical model explains the effect of microRNA-mediated synthetic genes regulation on intracellular resource allocation. *Nucleic Acids Res* **51**, 3452–3464 (2023).
21. Li, J. et al. Development and clinical advancement of small molecules for ex vivo expansion of hematopoietic stem cell. https://doi.org/10.1016/j.apsb.2021.12.006.
22. Zhang, H. et al. The magic of small-molecule drugs during ex vivo expansion in adoptive cell therapy. *Front. Immunol.* **14**, 1–10 (2023).
23. Banaszynski, L. A., Chen, L. C., Maynard-Smith, L. A., Ooi, A. G. & Wandless, T. J. A rapid, reversible, and tunable method to regulate protein function in living cells using synthetic small molecules. *Cell* **126**, 995–1004 (2006).
24. Xu, P., Xu, S., He, C. & Khetan, A. Applications of small molecules in modulating productivity and product quality of recombinant proteins produced using cell cultures. *Biotechnol. Adv.* **43**, 107577 (2020).
25. Rosa Silini, A. et al. Small molecule treatments improve differentiation potential of human amniotic fluid stem cells. https://doi.org/10.3389/fbioe.2021.623886 (2021).
26. Pavathuparambil, N. et al. An overview on small molecule-induced differentiation of mesenchymal stem cells into beta cells for diabetic therapy. https://doi.org/10.1186/s13287-019-1396-5.
27. Chang, J. et al. High-throughput screening identifies two novel small molecule enhancers of recombinant protein expression. *Molecules* **25**, 353 (2020).
28. Napolitano, F. et al. Automatic identification of small molecules that promote cell conversion and reprogramming. *Stem Cell Rep.* **16**, 1381–1390 (2021).
29. Keenan, A. B. et al. The library of integrated network-based cellular signatures NIH program: system-level cataloging of human cells response to perturbations. *Cell Syst.* **6**, 13–24 (2018).
30. Napolitano, F., Sirci, F., Carrella, D. & Di Bernardo, D. Drug-set enrichment analysis: a novel tool to investigate drug mode of action. *Bioinformatics* **32**, 235–241 (2016).
31. Muroski, M. E., Carnevale, K. J. F., Riskowski, R. A. & Strouse, G. F. Plasmid transfection in mammalian cells spatiotemporally tracked by a gold nanoparticle. *ACS Nano* **9**, 124–133 (2015).
32. Heine, A. et al. The JAK-inhibitor ruxolitinib impairs dendritic cell function in vitro and in vivo. *Blood* **122**, 1192–1202 (2013).

33. Chen, Y. Q. et al. Wnt pathway activator TWS119 enhances the proliferation and cytolytic activity of human γδT cells against colon cancer. *Exp. Cell Res.* **362**, 63–71 (2018).
34. Traves, P. G. et al. JAK selectivity and the implications for clinical inhibition of pharmacodynamic cytokine signalling by filgotinib, upadacitinib, tofacitinib and baricitinib. *Ann. Rheum. Dis.* **80**, 865–875 (2021).
35. Tan, S. et al. TIE2-high cervical cancer cells promote tumor angiogenesis by upregulating TIE2 and VEGFR2 in endothelial cells. *Transl. Oncol.* **26**, 101539 (2022).
36. Hackl, M. et al. Next-generation sequencing of the Chinese hamster ovary microRNA transcriptome: Identification, annotation and profiling of microRNAs as targets for cellular engineering. *J. Biotechnol.* **153**, 62–75 (2011).
37. Zhou, J. Y. et al. Analysis of microRNA expression profiles during the cell cycle in synchronized HeLa cells. *BMB Rep.* **42**, 593–598 (2009).
38. Sikora, M. et al. Comparison of selected non-coding RNAs and gene expression profiles between common osteosarcoma cell lines. *Cancers***14**, 1–19 (2022).
39. Nguyen, T. et al. Insights into CCL21's roles in immunosurveillance and immunotherapy for gliomas. *J. Neuroimmunol.* **305**, 29–34 (2017).
40. Transfiguracion, J. et al. Rapid in-process monitoring of lentiviral vector particles by high-performance liquid chromatography. *Mol. Ther. Methods Clin. Dev.* **18**, 803–810 (2020).
41. Cella, F., Wroblewska, L., Weiss, R. & Siciliano, V. Engineering protein-protein devices for multilayered regulation of mRNA translation using orthogonal proteases in mammalian cells. *Nat. Commun.* **9**, 4392 (2018).
42. Wroblewska, L. et al. Mammalian synthetic circuits with RNA binding proteins delivered by RNA. *Nat. Biotechnol.* **33**, 839–841 (2015).
43. Gabrielli, J., Blasi, R. Di, Kontoravdi, C. & Ceroni, F. Degradation bottlenecks and resource competition in transiently and stably engineered mammalian cells. *Nat. Commun.* **16**, 328 (2024).
44. Siciliano, V. et al. Construction and modelling of an inducible positive feedback loop stably integrated in a mammalian cell-line. *PLoS Comput. Biol.* **7**, e1002074 (2011).
45. Siciliano, V. et al. MiRNAs confer phenotypic robustness to gene networks by suppressing biological noise. *Nat. Commun.* **4**, 2364 (2013).
46. Schambach, A. et al. A new age of precision gene therapy. *Lancet* **403**, 568–582 (2024).
47. Earley, J., Piletska, E., Ronzitti, G. & Piletsky, S. Evading and overcoming AAV neutralization in gene therapy. *Trends Biotechnol.* **41**, 836–845 (2023).
48. Grimm, D. et al. In vitro and in vivo gene therapy vector evolution via multispecies interbreeding and retargeting of adeno-associated viruses. *J. Virol.* **82**, 5887–5911 (2008).
49. Gonzalez-Sandoval, A. et al. The AAV capsid can influence the epigenetic marking of rAAV delivered episomal genomes in a species dependent manner. *Nat. Commun.* **14**, 2448 (2023).
50. Benyamini, B., Esbin, M. N., Whitney, O., Walther, N. & Maurer, A. C. Transgene expression in cultured cells using unpurified recombinant adeno-associated viral vectors. *J. Vis. Exp.* **2023**, (2023).
51. Malm, M. et al. Harnessing secretory pathway differences between HEK293 and CHO to rescue production of difficult to express proteins. *Metab. Eng.* **72**, 171–187 (2022).
52. Hu, X., li, J., Fu, M., Zhao, X. & Wang, W. The JAK/STAT signaling pathway: from bench to clinic. *Signal Transduct. Target. Ther.* **6**, 402 (2021).
53. Au-Yeung, N., Mandhana, R. & Horvath, C. M. Transcriptional regulation by STAT1 and STAT2 in the interferon JAK-STAT pathway. *Jak. -Stat.* **2**, e23931 (2013).
54. Kim, E. S. & Keam, S. J. Filgotinib in rheumatoid arthritis: a profile of its use. *Clin. Drug Investig.* **41**, 741–749 (2021).
55. Borkowski, O., Ceroni, F., Stan, G. B. & Ellis, T. Overloaded and stressed: whole-cell considerations for bacterial synthetic biology. *Curr. Opin. Microbiol.* **33**, 123–130 (2016).
56. Barajas, C., Huang, H. H., Gibson, J., Sandoval, L. & Del Vecchio, D. Feedforward growth rate control mitigates gene activation burden. *Nat. Commun.* **13**, 1–10 (2022).
57. Martella, A., Matjusaitis, M., Auxillos, J., Pollard, S. M. & Cai, Y. EMMA: an extensible mammalian modular assembly toolkit for the rapid design and production of diverse expression vectors. *ACS Synth. Biol.* **6**, 1380–1392 (2017).
58. Auricchio, A., Hildinger, M., O'Connor, E., Gao, G. P. & Wilson, J. M. Isolation of highly infectious and pure adeno-associated virus type 2 vectors with a single-step gravity-flow column. *Hum. Gene Ther.* **12**, 71–76 (2001).
59. Dobin, A. et al. STAR: ultrafast universal RNA-seq aligner. *Bioinformatics* **29**, 15–21 (2013).
60. Anders, S., Pyl, P. T. & Huber, W. HTSeq-A Python framework to work with high-throughput sequencing data. *Bioinformatics* **31**, 166–169 (2015).
61. Robinson, M. D., McCarthy, D. J. & Smyth, G. K. edgeR: a bioconductor package for differential expression analysis of digital gene expression data. *Bioinformatics* **26**, 139–140 (2009).
62. Wu, T. et al. clusterProfiler 4.0: A universal enrichment tool for interpreting omics data. *Innovation* **2**, 100141 (2021).
63. Napolitano, F., Carrella, D., Gao, X. & di Bernardo, D. gep2pep: a bioconductor package for the creation and analysis of pathway-based expression profiles. *Bioinformatics* **36**, 1944–1945 (2020).
64. Liberzon, A. et al. The molecular signatures database (MSigDB) hallmark gene set collection. *Cell Syst.* **1**, 417–425 (2016).

Acknowledgements

We thank Daniela Perna for technical support. We thank the genomics facility at IIT for the support on the RNA sequencing. FUNDING**:** ERC Starting grant Synthetic T-rex [852012]; NextGenerationEU PNRR MUR [M4C2]; National Center for Gene Therapy and Drugs based on RNA Technology [CN00000041]. A.C. was supported by the Italian Ministry of Research under the complementary actions to the NRRP "D34Health —Digital Driven Diagnostics, prognostics and therapeutics for sustainable Health care" Grant (PNC0000001).

Author contributions

V.S. conceived the project, V.S. and M.P. designed experiments. M.P. performed the experiments. F.C. performed the transfection for RNA-sequencing. F.CA. designed and produced the modified RNA. I.B. and N.B.P. produced the AAV vectors. A.R. analyzed the RNA-seq data and provided bioinformatics support. A.C., M.P., and V.S. analyzed the data. A.C. performed statistical analysis. D.V. performed the RNA sequencing. F.T. performed experiments in integrated cell lines. F.N. performed the computational work. V.S. supervised the experimental work and secured funding. M.P., F.N., A.R., and V.S. wrote the manuscript. F.C., A.C., V.S. edited the manuscript.

Competing interests

The authors declare no competing interests.

Additional information

Supplementary information The online version contains supplementary material available at https://doi.org/10.1038/s41467-025-62529-9.

Correspondence and requests for materials should be addressed to V. Siciliano.

Peer review information *Nature Communications* thanks Xinyi Wang and the other, anonymous, reviewer(s) for their contribution to the peer review of this work. A peer review file is available.